Title

Understanding Diameter and Length Effects in a Solution-Processable Tellurium-Poly(3,4-Ethylenedioxythiophene) Polystyrene Sulfonate Hybrid Thermoelectric Nanowire Mesh

Journal

Advanced Electronic Materials, 7(3)

ISSN

2199-160X

Authors

Gordon, Madeleine P
Haas, Kyle
Zaia, Edmond
et al.

Publication Date

2021-03-01

DOI

10.1002/aelm.202000904

Peer reviewed

ADVANCED ELECTRONIC MATERIALS
www.advelectronicmat.de

Understanding Diameter and Length Effects in a Solution-Processable Tellurium-Poly(3,4-Ethylenedioxythiophene) Polystyrene Sulfonate Hybrid Thermoelectric Nanowire Mesh

*Madeleine P. Gordon, Kyle Haas, Edmond Zaia, Akanksha K. Menon, Lin Yang, Alexandra Bruefach, Michael D. Galluzzo, Mary C. Scott, Ravi S. Prasher, Ayaskanta Sahu, and Jeffrey J. Urban**

Organic–inorganic hybrids offer great promise as solution-processable thermoelectric materials. However, they have struggled to surpass the performance of their rigid inorganic counterparts due, in part, to a lack of synthetic control and limited understanding of how inorganic nanostructure dimensions impact overall charge transport. While it has been hypothesized that length, diameter, and aspect ratio (AR) all impact electronic transport in hybrid nanowires, the field lacks clarity on the relative role of each. In this study, the experimental parameter of ligand molecular weight (MW) is investigated as a synthetic knob for modulating nanowire dimensions, as well as the deconvolution of nanowire length versus diameter impacts on electron transport. By increasing ligand MW, larger nanowire AR dispersions occur and an optimal power factor of ≈130 μWm^{-1} K^{-2} is achieved for a modest AR of 73. Power factors of this magnitude are thought to only be achievable in ultrahigh AR systems; representing a 183% increase in performance over literature reports with similar AR. Additionally, nanowire diameter is demonstrated to be a far more sensitive parameter for enhancing performance than modulating length. This study provides improved fundamental insight into rational synthetic design avenues for future enhancements in the performance of hybrid materials.

Hybrid thermoelectrics (TEs) are attractive as they combine the low thermal conductivity and solution processability of organic materials with the structural and electronic tunability of inorganic nanostructures.[1–3] These materials enable the realization of flexible and printable novel devices that can harness unconventional heat sources, such as body heat, to generate electricity or provide solid-state cooling with the promise of cost-effective solution-based manufacturing.[1,2,4–9] The true sign of a hybrid material is significantly enhanced performance as a result of non-linear interactions that occur at the nanoscale interfacial layer formed between the two constituents.[8–11] This results in a new material class that offers tunable material interfaces with performance otherwise unattainable within simple composites.[10,12]

M. P. Gordon
Applied Science and Technology Graduate Group
University of California
Berkeley, CA 94720, USA

M. P. Gordon, K. Haas, Dr. E. W. Zaia, Prof. A. Sahu, Dr. J. J. Urban
The Molecular Foundry
Lawrence Berkeley National Laboratory
Berkeley, CA 94720, USA
E-mail: jjurban@lbl.gov

K. Haas
College of Engineering
University of California
Berkeley, CA 94720, USA

The ORCID identification number(s) for the author(s) of this article can be found under https://doi.org/10.1002/aelm.202000904.

DOI: 10.1002/aelm.202000904

Dr. E. W. Zaia, M. D. Galluzzo
Department of Chemical and Biomolecular Engineering
University of California Berkeley
Berkeley, CA 94720, USA

Dr. A. K. Menon, Dr. L. Yang, Prof. R. S. Prasher
Energy Storage and Distributed Resources Division
Lawrence Berkeley National Laboratory
Berkeley, CA 94720, USA

A. Bruefach, Prof. M. C. Scott
Department of Materials Science and Engineering
University of California
Berkeley, CA 94720, USA

A. Bruefach, Prof. M. C. Scott
National Center for Electron Microscopy, The Molecular Foundry
Lawrence Berkeley National Laboratory
Berkeley, CA 94720, USA

Prof. R. S. Prasher
Department of Mechanical Engineering
University of California
Berkeley, CA 94720, USA

The performance of a TE material is characterized by a dimensionless figure of merit, $ZT = \frac{(S^2\sigma)}{\kappa} \times T$, comprised of its Seebeck coefficient, S; electrical conductivity, σ; thermal conductivity, κ; and the absolute temperature, T. The quantity $S^2\sigma$ is known as the power factor and denotes the electronic performance of the TE material. The most widely studied hybrid material is tellurium (Te) nanowires (NWs) coated with poly(3,4-ethylenedioxythiophene) polystyrene sulfonate (PEDOT:PSS). This Te–PEDOT:PSS system effectively leverages the high electrical conductivity of PEDOT:PSS and a high Seebeck coefficient attributed to Te, to achieve power factors of ≈145 $\mu W m^{-1} K^{-2}$ for NWs with ultrahigh aspect ratios (AR = length, L/diameter, D) ≈1000 without any extrinsic doping.[10]

Typically, high ARs are achieved by dramatically increasing NW length which leads to a decrease in interfacial scattering events.[10,13,14] However, diameter also often changes in these studies, so it is unclear whether length or diameter is the true driving force behind the observed performance enhancements. Recent studies have shown that charge transport is dominated by the organic phase within the Te–PEDOT:PSS hybrid NW, and the improvement in TE performance is attributed to the interaction of the polymer with the inorganic NW surface.[11] This interaction results in the self-assembly (alignment or templating) of the polymer along the crystalline facets of the inorganic NW, which is governed by differences in surface energy at the hard–soft interface.[11] It is well-established that surface energy has a size dependence,[15,16] however, to date, little work has been done to explore the role of NW diameter and length in enhancing the performance of hybrid TE materials.

A study by Yee et al. attempted to deconvolute the contributions of NW length and diameter on the TE properties of these hybrid bulk films, but were unable to effectively separate the effects due to a lack of synthetic control with the standard one-pot Te–PEDOT:PSS NW synthesis.[17] Te–PEDOT:PSS NWs have traditionally been synthesized exclusively with PEDOT:PSS as the nucleation directing surface ligand.[8,17–19] Given that PEDOT:PSS is a commercial polymer blend, the tunability and control of such a synthesis is limited.[17] An alternative approach for synthesizing Te NWs uses polyvinylpyrrolidone (PVP) as the surface ligand,[20–23] and this has been shown to provide added degrees of synthetic control in other analogous NW systems.[24–26] For example, Zeng et al. demonstrated that well-defined high AR silver NWs could be synthesized by modulating PVP molecular weight (MW).[27] While PVP is not an optimal polymer coating for Te NWs owing to its electrically insulating nature, it imparts synthetic tunability as a myriad of PVP MWs are commercially available.[28,29] Sahu et al. proposed a synthetic process for ligand exchange that is tailored specifically to converting NWs of Te–PVP to Te–PEDOT:PSS, which are of interest for TE applications.[10,30]

Herein for the first time, we vary the ligand MW to study its effect on Te NW size, as well as the TE performance of the resulting Te–PEDOT:PSS NWs post ligand exchange. We find that increased PVP MW results in larger NW AR dispersions where NW length remains relatively constant but diameter decreases, and an optimal power factor of 130 $\mu W mK^{-2}$ is achieved at a modest AR of 73. Such high performance is in contrast with previous reports of the same hybrid material synthesized via different means, wherein an ultrahigh AR of ≈1000 was required for a comparable power factor.

The synthesis used in this work is depicted in **Figure 1**a, which yields NWs of uniform surface morphologies as shown in Figure 1b. Figure 1c shows a high-resolution transmission electron microscopy (HRTEM) micrograph of the core–shell structure of the PVP polymer coating the Te crystalline core prior to the ligand exchange.

Three different PVP MWs were used in the NW synthesis (29, 40, and 55 kDa) to produce batches of Te NWs with PVP as the surface ligand that are referred to as PVP-29, PVP-40, and PVP-55. ln the next step, the system undergoes a series of ligand exchanges (Figure 1a), to yield a hybrid material predominantly composed of a Te NW core encapsulated by the conducting polymer PEDOT:PSS shell (Figure 1c). This ligand exchange process does not always result in samples with exactly the same ratios of inorganic to organic constituents, thus organic to inorganic weight percent was corrected by adding excess PEDOT:PSS and quantified via thermogravimetric analysis (TGA, Figure S1, Supporting Information). The different batches of NWs synthesized were found to have differing diameters and roughly constant lengths owing to the use of different PVP MWs. As shown in **Table 1**, PVP of different MWs results in a large range of NW diameters but a small range of lengths, ultimately yielding different ARs. The results tabulated in Table 1 are displayed in histogram form in Figures S2–S4, Supporting Information. PVP-40 clearly demonstrates the smallest average diameter size and tightest size distribution.

Inspection of SEM panels a, b, and c in **Figure 2** illustrate the visual differences that arise between each system. Powder X-ray diffraction (PXRD) run on each of the film sets confirms that the NW cores are entirely composed of Te and that the inorganic trigonal crystal structure is consistent between batches, Figure 2d.

Insight into the cause for increase in ARs as a function of PVP MW can be explained using a study performed by Xu et al. that provides a careful analysis of the nucleation dynamics of PVP with respect to the Te surface.[26] They estimate binding energy preferences of PVP to certain crystal planes of Te according to a theoretical framework established by Fichthorn et al. and find a linear correlation between increasing number of PVP monomer units and an increasing preference for binding onto the (100) and (101) planes rather than the (001) plane.[31] Thus, suggesting that for larger PVP MWs there is less of a likelihood for a PVP unit to bind to the (001) plane (the plane perpendicular to and intersecting with the axial direction of growth) that ultimately leads to larger AR NWs. While Xu et al. did not experimentally observe a dramatic difference in NW dimensions when using different PVP MWs, their synthetic process is carried out in water as opposed to ethylene glycol (EG) (which was used in this study), therefore it is possible that differences in solvent viscosity alter the nucleation kinetics between their findings and the current work.

In an attempt to further elucidate the underlying factors at play, gel permeation chromatograph (GPC) was run on the PVP

Prof. A. Sahu
Department of Chemical and Biomolecular Engineering
New York University
Brooklyn, NY 11201, USA

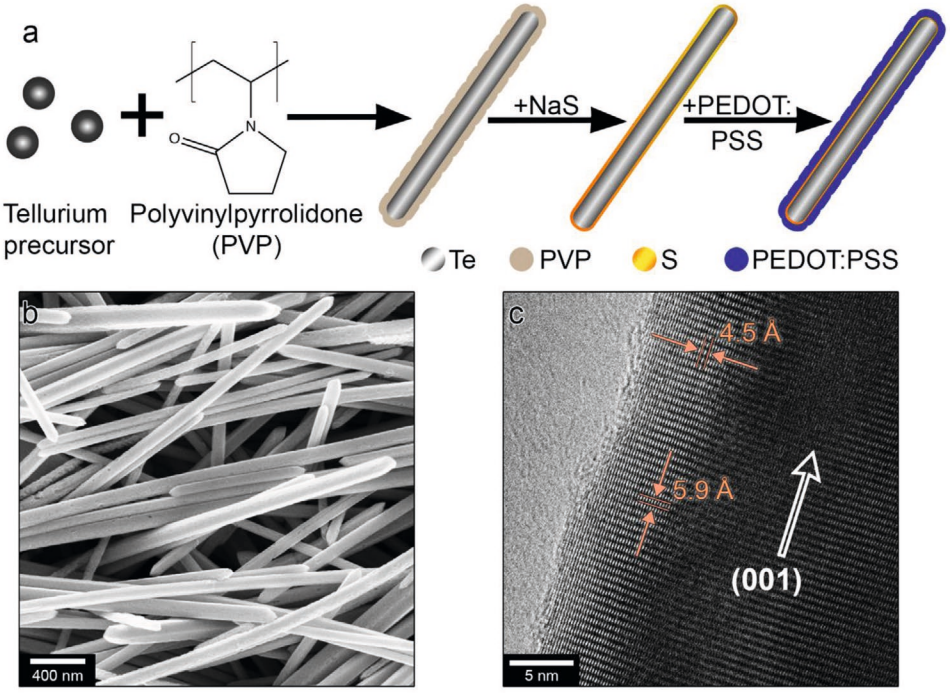

Figure 1. Depiction of the synthetic process employed, paired with SEM and HRTEM micrographs depicting the structure of the Te–PVP coated NWs. a) A general cartoon schematic of the multistep synthetic process for forming the hybrid nanostructures. b) A representative scanning electron micrograph shows the microscale morphology of the Te–PVP NWs. c) A representative transmission electron micrograph of the Te–PVP wire which shows the thin polymer layer on the surface of the inorganic core and distinctly shows the lattice fringes indicative of atomic spacings in the unit cell.

starting polymers in order to confirm the MW and polydispersity index (D) of the polymers. The GPC results are detailed in Table S1, Supporting Information, and demonstrate that the actual differences between the claimed MWs are closer than the nominal values. In particular, the GPC results indicate that the 55 kDa PVP is only slightly higher in MW than the 40 kDa. Thus, the similarities in AR between these two systems are not surprising.

Sahu et al. employed the PVP-based multistep synthetic method and modulated reagent concentrations to synthesize two sets of NWs with different ARs, 20 and 1000, and a diameter held constant at ≈25 nm, resulting in TE power factors of 25 and 145 $\mu Wm^{-1} K^{-2}$, respectively.[10] Instead, by using different PVP MW in the synthesis, we observe that similar power factors can be attained at lower ARs. **Figure 3**a,b shows the TE properties of PVP-29, PVP-40, and PVP-55 as a function of the average AR for each hybrid; the Seebeck coefficient does not show a strong dependence on AR but electrical conductivity does increase as AR increases. The highest AR is obtained in PVP-40, which shows the highest electrical conductivity, and this performance enhancement translates to a power factor of ≈127 $\mu Wm^{-1} K^{-2}$ for a hybrid with no extrinsic doping. The benefit of achieving such high power factors in an undoped material is the possibility for future performance enhancement through utilization of well-established doping/de-doping protocols in literature.[8,10,17,32] These materials far exceed the performance of Te–PEDOT:PSS hybrids reported in literature with comparable or smaller ARs, and rivals the power factor reported by Sahu et. al. for the same material at an ultrahigh AR of ≈1000.[10] A comparison of power factors and ARs (calculated from the reported NW dimensions in each paper) for the hybrid NWs presented in this work and those reported in literature are shown in Table S2, Supporting Information.[10,17–19,32]

Table 1. Diameter, length, and aspect ratio for Te NWs synthesized using different PVP MWs, as determined by SEM for $n > 50$ NWs of each kind.

Sample	Diameter [nm]	Length [μm]	Aspect Ratio
PVP-29	109 (±84)	4.6 (±2.3)	42
PVP-40	56.9 (±16)	4.2 (±1.6)	73
PVP-55	83.0 (±50)	5.6 (±3.2)	68

With this PVP MW modulating technique, the NWs produced are similar in length, which implies that NW diameter is the main driver impacting charge transport. Figure 3c,d shows electrical conductivity (the parameter most dramatically impacted by AR) as a function of NW length and diameter, respectively. While Figure 3c does not show a distinct trend, Figure 3d shows a direct correlation between decreasing diameter and increased conductivity. Figure S5, Supporting Information, shows power factor as a function of both NW diameter and length. We observe a power factor enhancement from 40 to 127 $\mu Wm^{-1} K^{-2}$ as a result of average diameter decrease from 110 to 57 nm for PVP-29 and PVP-40, respectively. Reducing the NW diameter by 3x brings about roughly the same performance enhancement as that observed by Sahu et al. for a 100× increase in NW length. Thus, it appears that TE performance is significantly more sensitive to NW diameter differences than changes in NW length.

This diameter dependent conductivity result is also consistent with our recent study on single NWs of Te–PEDOT:PSS with the same synthesis method as this work using the 40 kDa

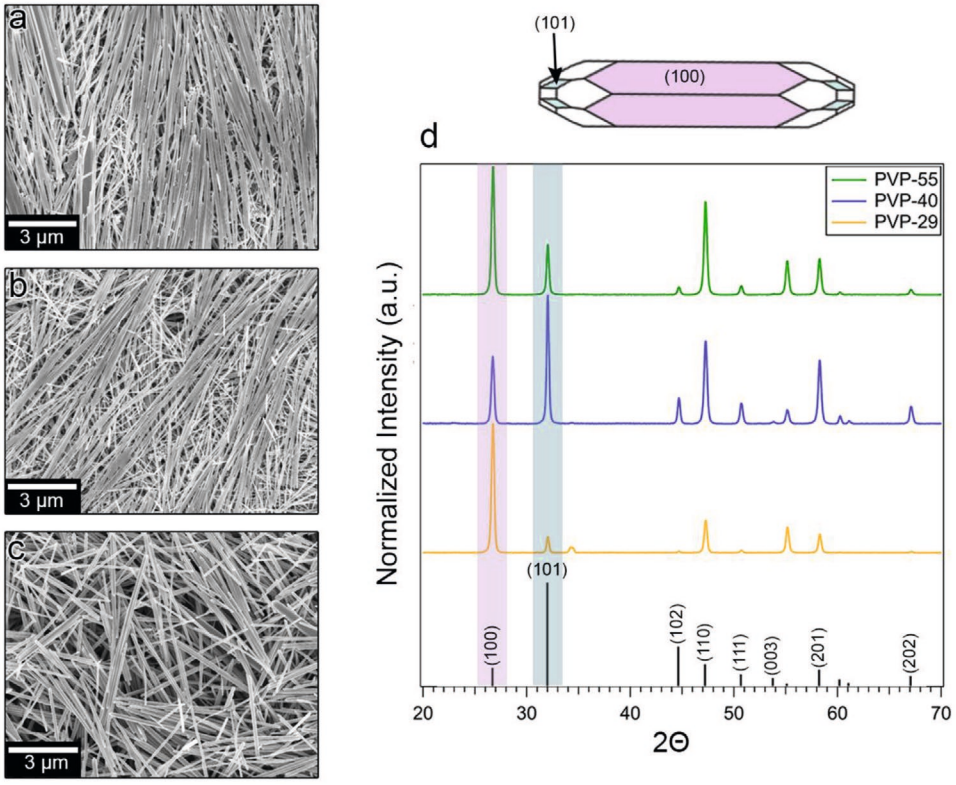

Figure 2. Scanning electron micrographs and powder X-ray diffraction (PXRD) for Te NWs synthesized with three different molecular weights of PVP show a clear trend of increasing AR distribution as a function of PVP molecular weight increase. a) Corresponds to PVP-29 wires, b) PVP-40 NWs, and c) PVP-55 NWs. d) Provides clear confirmation that all the Te NW batches are of the same trigonal crystal structure belonging to space group P3121. Above (d) a visual representation of the Te NW facets can be found where the body facet (100) is marked in pink and the end facet (101) is highlighted in blue.

PVP.[33] It is observed that electrical conductivity monotonically increases as NW diameter decreases, while the Seebeck coefficient remains relatively constant. This enhancement is attributed to increased mobility arising from templating of PEDOT:PSS on the surface of the inorganic NW, as there is a decrease in surface energy for smaller wire diameters that enables the polymer chains to align or self-assemble on the Te NW surface.[33] These findings paired with the results discussed in this study suggest that nanoscale templating effects dependent on NW diameter impact overall transport far more than macroscale interfacial scattering that is dominated by NW length.

In conclusion, this report explored the morphological impacts of utilizing different MWs of surface ligand PVP and provided some insight on the fundamental driving forces behind the TE performances observed in the resulting hybrid systems. We demonstrate a power factor of ≈130 $\mu W m^{-1} K^{-2}$ for our entirely undoped and untreated low AR Te–PEDOT:PSS NWs, which rivals the high performances of the same materials with ultrahigh ARs. This comparable performance for dramatically different ARs demonstrates the need to further decouple effects of NW length and diameter. This work challenges traditional design rules (i.e., high ARs) thought to be necessary for high TE performance in this hybrid system and instead posits that average NW diameter dominates charge transport within the system. This in turn will guide the rational design of next generation high performing hybrid materials in order to realize their potential in devices for a wide array of energy harvesting applications.

Experimental Section

Nanowire Synthesis: PEDOT:PSS (Clevios PH1000) was purchased from Heraeus and underwent no further processing other than vortexing and filtration. Tellurium dioxide (99.9995%), PVP (average MWs 29, 40, and 55 kDa), sodium hydroxide (NaOH, ACS reagent, ≥97.0%, pellets), EG (ReagentPlus, ≥99%), hydrazine hydrate (HH, 78–82%, iodometric), and sodium sulfide (NaS) were purchased from Sigma Aldrich.

Tellurium–Polyvinylpyrrolidone Nanowires: Synthesis of PVP coated Te NWs and the necessary ligand exchange process followed protocol established in existing literature, barring some slight modification.[10] In this reaction EG (30 mL) was utilized as both the solvent and as the partial reducing agent. EG was placed in a round bottom flask under an inert N_2 environment, stirred with a Teflon stir bar and its temperature was monitored by thermocouple. NaOH (0.9 g) was then slowly added to the EG solution and allowed to stir until fully dissolved. Upon dissolution of NaOH in the mixture, PVP (0.3 g) was added and dissolved. The same was done for the addition of TeO_2 (0.72 g). Once all of these reagents had been added, then a heating mantle was placed beneath the round bottom flask and the solution was slowly heated to 160 °C and vented while maintaining stirring and inert environment conditions. The solution initially appeared translucent but as heating continues, it transitioned to a clear yellow before becoming dark and opaque. The appearance of a dark grey/brown opaque color was indicative of the start of nucleation. When the solution temperature approached 160 °C then HH (1.5 mL) should be rapidly injected into the mixture in order to truly induce nucleation. Once HH had been injected the reaction was left to heat and stirred for 1 h. The reaction was then quenched by removing the heat source and submerging the round bottom flask into a cool water bath. Once the product temperature had lowered to ≈35 °C then the contents of the flask were transferred to 50 mL disposable Falcon

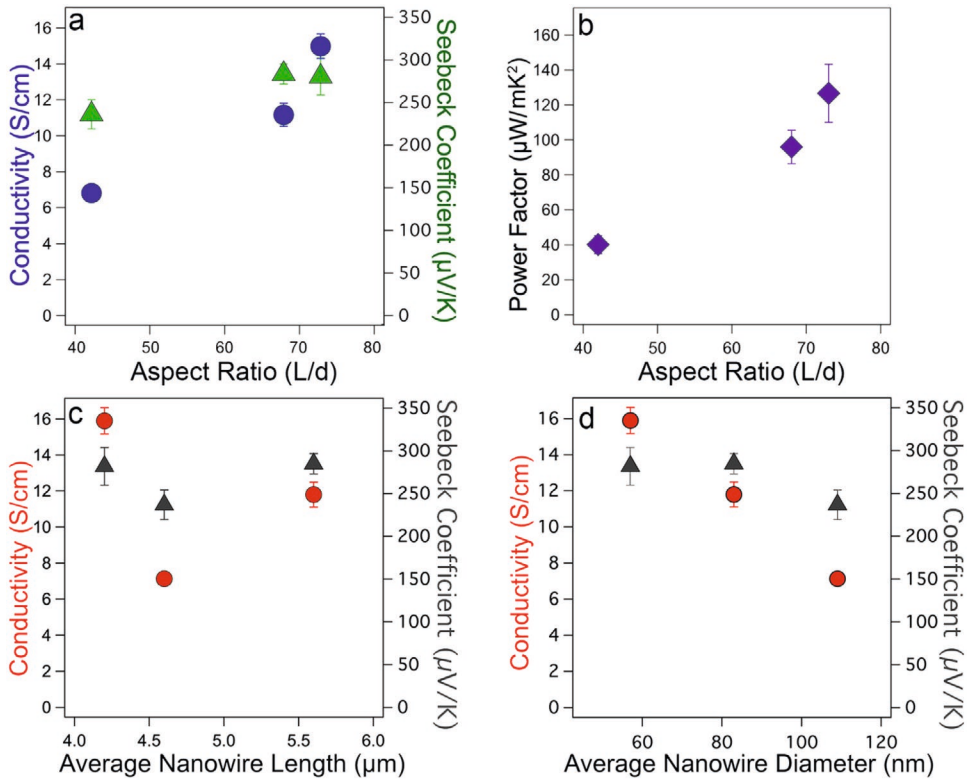

Figure 3. Thermoelectric performances of the as-synthesized Te–PEDOT:PSS NWs. a,b) Electrical conductivity, Seebeck coefficient, and power factor are shown in graphs as a function of AR. There appears to be a clear correlation between AR and performance where the highest performing set of wires having an AR of 73, demonstrate a power factor of ≈130 μW mK^{-2}. In order to better understand the driving forces behind this trend, conductivity and Seebeck coefficient as a function of average c) NW length and d) diameter are shown. While there is a distinct lack of trend between conductivity and NW length, a dependency can be observed as a function of NW diameter. Vertical errors bars are the standard deviations between triplicate measurements.

tubes to prepare for the cleaning process. To clean the NW solution, the tubes were centrifuged for 35 min at 9000 rpm, then the supernatant was poured off, fresh deionized water was added, and the entire tube was vortexed. This process was repeated 5–6 times or until the supernatant appeared clear then the final cleaned Te–PVP wires bound in the bottom pellet were resuspended in water.

Tellurium–Poly(3,4-ethylenedioxythiophene) Polystyrene Sulfonate Nanowires: In order to convert the Te–PVP NWs to the more useful form of Te–PEDOT:PSS NWs, a multistep ligand exchange process was employed. The cleaned Te–PVP NWs were placed in a closed jar with excess water and NaS (≈1 g). The mixture was left to stir overnight. The next morning the NW solution was cleaned thrice following the same centrifugation protocol detailed above. The cleaned NWs were then suspended in excess water and PEDOT:PSS (≈10 mL) was added to the solution. The mixture was again stirred and left overnight. After stirring overnight, the PEDOT:PSS-NW solution was cleaned again thrice via centrifugation to yield clean Te–PEDOT:PSS NWs.

Thin Film Preparation: Thin film samples were prepared by employing a drop cast technique onto glass substrates (9.5 mm × 9.5 mm, 1 mm thick–thin film devices). The substrates were prepared for deposition by undergoing UV–ozone treatment for at least 10 min prior to casting. Once clean, the substrates were placed upon a hot plate and heated at 90 °C; then 75 μL of the hybrid NW composite solution was deposited and left to dry for 10–20 min until solvent was entirely gone. 100 nm gold contacts were thermally evaporated onto each of the four corners of the thin films using a shadow mask to aid in electrical contact during TE measurements.

Electrical and Thermoelectric Measurements: Keithley 2400 Source meters in four-probe van-der-Pauw configuration were used to measure the sheet resistance of each film. The thickness of each film was measured by measuring the step height of a scratched film using a Veeco Dektak 150 profilometer. Electrical conductivity values were then calculated using the sheet resistance and the thickness measurements. The Seebeck coefficient was determined using a homemade probe setup consisting of two Peltier devices (Ferrotec) placed ≈4 mm apart. A single current was passed through each of the Peltier devices in opposite directions, resulting in one device heating up and the other cooling in roughly the same amount with respect to room temperature. A thin film sample was then suspended across the gap between the two Peltier devices (thermal paste was utilized to ensure good thermal contact was being made—Wakefield Thermal S3 Solutions) in order to enable a thermal gradient to arise. The open circuit voltage was then measured across the sample in the same direction as the temperature gradient using an Agilent 34401 multimeter. The magnitude of the temperature gradient across the sample was monitored by the placement of two T-type thermocouples mounted in micromanipulators. The magnitude of the temperature gradient was directly related to the magnitude of current driven through the Peltier devices, thus five different temperature gradients were established (200 s equilibration time allowance between each temperature gradient). Ten voltage measurements were taken and averaged at each chosen gradient point. All samples exhibited linear variation of open circuit voltage with temperature gradient; this trend was then used to extract Seebeck coefficient values. Data for both electrical conductivity and Seebeck coefficient were acquired using homemade Labview programs. For each measurement, at least three different samples were measured and averaged, with error bars representing standard error. Ohmic contacts were confirmed before measurements.

Characterization: Scanning electron microscopy (SEM), transmission electron microscopy (TEM), X-Ray diffraction (XRD), and TGA were used to characterize the size, shape, structure, and composition of the composite system.

Scanning Electron Microscopy: SEM images were captured on a Zeiss Gemini Ultra55 analytical field emission scanning electron microscope using beam energy of 5 kV.

Transmission Electron Microscopy: A FEI monochromated F20 UT Tecnai was operated at an accelerating voltage of 200 kV. Real space images were taken with a spot size of 3 and an exposure of 0.7 s. TEM samples were prepared by placing a TEM grid (400-mesh Cu on holey carbon—Ted Pella 01824) on a filter paper taped flat to a hot plate at 90 °C. A single drop of dilute hybrid material solution was deposited onto the grid and then water was slowly forced off for 5 min.

X-Ray Diffraction: A Bruker AXS D8 Discover GADDS XRD micro-diffractometer was used to capture wide-angle spectra using a 0.154 nm wavelength Cu-Kα source.

Thermogravimetric Analysis: To quantify the organic–inorganic weight percent ratio of each sample, a TA Instruments Q5000IR TGA was used. 7–10 mg of each sample was ramped to 600 °C at a heating rate of 10 °C min^{-1} and then it underwent an isothermal hold of 60 min in order to guarantee complete organic phase decomposition. The total mass percent change after this process was assumed to be the organic component of the hybrid composite system where as the remaining weight percent was assumed to be the inorganic component.

Gel Permeation Chromatography: GPC was conducted on an Agilent 1260 Infinity Series fitted with Waters Styragel HR3 and HR4 columns with 0.05 M LiBr in *N*-methyl-2-pyrrolidone (NMP) as the mobile phase. The GPC was calibrated using poly(ethylene oxide) standards. The polymer samples were mixed with NMP and stirred at 60 °C until clear solutions were formed and then passed through a 2-µm filter before analysis.

Supporting Information

Supporting Information is available from the Wiley Online Library or from the author.

Acknowledgements

This work was performed at the Molecular Foundry, Lawrence Berkeley National Laboratory, and was supported by the Department of Energy, Office of Science, Office of Basic Energy Sciences, Scientific User Facilities Division of the U.S. Department of Energy under Contract No. DE-AC02-05CH11231. M.P.G. gratefully acknowledges the National Science Foundation for fellowship support under the National Science Foundation Graduate Research Fellowship Program. A.K.M. acknowledges funding support from the ITRI-Rosenfeld Fellowship from the Energy Technologies Area at Lawrence Berkeley National Laboratory.

Conflict of Interest

The authors declare no conflict of interest.

Keywords

hybrids, nanowires, nanowire meshes, organic–inorganic hybrids, thermoelectrics

Received: September 11, 2020
Revised: December 7, 2020
Published online:

[1] E. W. Zaia, M. P. Gordon, P. Yuan, J. J. Urban, *Adv. Electron. Mater.* **2019**, *5*, 1800823.
[2] B. Russ, A. Glaudell, J. J. Urban, M. L. Chabinyc, R. A. Segalman, *Nat. Rev. Mater.* **2016**, *1*, 16050.
[3] D. Patidar, N. S. Saxena, *Adv. Nanopart.* **2013**, *2*, 11.
[4] J. J. Urban, A. K. Menon, Z. Tian, A. Jain, K. Hippalgaonkar, *J. Appl. Phys.* **2019**, *125*, 180902.
[5] H. M. Elmoughni, A. K. Menon, R. M. W. Wolfe, S. K. Yee, *Adv. Mater. Technol.* **2019**, *4*, 1800708.
[6] A. K. Menon, S. K. Yee, *J. Appl. Phys.* **2016**, *119*, 055501.
[7] K. Gordiz, A. K. Menon, S. K. Yee, *J. Appl. Phys.* **2017**, *122*, 124507.
[8] E. W. Zaia, A. Sahu, P. Zhou, M. P. Gordon, J. D. Forster, S. Aloni, Y.-S. Liu, J. Guo, J. J. Urban, *Nano Lett.* **2016**, *16*, 3352.
[9] E. W. Zaia, M. P. Gordon, V. Niemann, J. Choi, R. Chatterjee, C.-H. Hsu, J. Yano, B. Russ, A. Sahu, J. J. Urban, *Adv. Energy Mater.* **2019**, *9*, 1803469.
[10] A. Sahu, B. Russ, N. C. Su, J. D. Forster, P. Zhou, E. S. Cho, P. Ercius, N. E. Coates, R. A. Segalman, J. J. Urban, *J. Mater. Chem. A* **2017**, *5*, 3346.
[11] P. Kumar, E. W. Zaia, E. Yildirim, D. V. M. Repaka, S.-W. Yang, J. J. Urban, K. Hippalgaonkar, *Nat. Commun.* **2018**, *9*, 5347.
[12] E. S. Cho, N. E. Coates, J. D. Forster, A. M. Ruminski, B. Russ, A. Sahu, N. C. Su, F. Yang, J. J. Urban, *Adv. Mater.* **2015**, *27*, 5744.
[13] Q. Xue, W. Yao, J. Liu, Q. Tian, L. Liu, M. Li, Q. Lu, R. Peng, W. Wu, *Nanoscale Res. Lett.* **2017**, *12*, 480.
[14] L. Sonntag, F. Eichler, N. Weiß, L. Bormann, D. S. Ghosh, J. M. Sonntag, R. Jordan, N. Gaponik, K. Leo, A. Eychmüller, *Phys. Chem. Chem. Phys.* **2019**, *21*, 9036.
[15] G. Ouyang, X. L. Li, X. Tan, G. W. Yang, *Nanotechnology* **2008**, *19*, 045709.
[16] P. Ghosh, M. U. Kahaly, U. V. Waghmare, *Phys. Rev. B* **2007**, *75*, 245437.
[17] S. K. Yee, N. E. Coates, A. Majumdar, J. J. Urban, R. A. Segalman, *Phys. Chem. Chem. Phys.* **2013**, *15*, 4024.
[18] K. C. See, J. P. Feser, C. E. Chen, A. Majumdar, J. J. Urban, R. A. Segalman, *Nano Lett.* **2010**, *10*, 4664.
[19] N. E. Coates, S. K. Yee, B. McCulloch, K. C. See, A. Majumdar, R. A. Segalman, J. J. Urban, *Adv. Mater.* **2013**, *25*, 1629.
[20] X. Chen, Z. Wang, X. Wang, J. Wan, Y. Qian, *Appl. Phys. A* **2005**, *80*, 1443.
[21] B. Kim, B.-K. Park, *Electron. Mater. Lett.* **2012**, *8*, 33.
[22] H. Dong, Y.-C. Chen, C. Feldmann, *G. Chem.* **2015**, *17*, 4107.
[23] Y.-J. Zhu, X.-L. Hu, W.-W. Wang, *Nanotechnology* **2006**, *17*, 645.
[24] Z. Liu, Z. Hu, Q. Xie, B. Yang, J. Wu, Y. Qian, *J. Mater. Chem.* **2003**, *13*, 159.
[25] F. Liang, H. Qian, *Mater. Chem. Phys.* **2009**, *113*, 523.
[26] L. Xu, G. Wang, X. Zheng, H. Pan, J. Zhu, Z. Li, S.-H. Yu, *Chem* **2018**, *4*, 2451.
[27] X. Zeng, B. Zhou, Y. Gao, C. Wang, S. Li, C. Y. Yeung, W. Wen, *Nanotechnology* **2014**, *25*, 495601.
[28] F.-Y. Yang, K.-J. Chang, M.-Y. Hsu, C.-C. Liu, *J. Mater. Chem.* **2008**, *18*, 5927.
[29] S. K. S. Basha, G. S. Sundari, K. V. Kumar, M. C. Rao, *J. Inorg. Organomet. Polym. Mater.* **2017**, *27*, 455.
[30] A. Sahu, B. Russ, M. Liu, F. Yang, E. W. Zaia, M. P. Gordon, J. D. Forster, Y.-Q. Zhang, M. C. Scott, K. A. Persson, N. E. Coates, R. A. Segalman, J. J. Urban, *Nat. Commun.* **2020**, *11*, 2069.
[31] K. A. Fichthorn, T. Balankura, X. Qi, *CrystEngComm* **2016**, *18*, 5410.
[32] E. J. Bae, Y. H. Kang, K.-S. Jang, S. Y. Cho, *Sci. Rep.* **2016**, *6*, 18805.
[33] L. Yang, M. P. Gordon, A. K. Menon, A. Bruefach, K. Haas, M. C. Scott, R. S. Prasher, J. J. Urban, unpublished.